Layer Rigidity and Collective Effects in Pillared Lamellar Solids

H. Kim,[a] W. Jin,[b] S. Lee,[b] P. Zhou,[b] T. J. Pinnavaia,[a] S. D. Mahanti,[b] and S. A. Solin[b]
Center for Fundamental Materials Research, Michigan State University, East Lansing, Michigan 48824
(Received 18 November 1987)

The x dependence of the normalized basal spacing, $d_n(x)$, of pillared vermiculite (Vm) has been measured for the mixed-layer system $[(CH_3)_4N^+]_x[(CH_3)_3NH^+]_{1-x}$-Vm and compared with that of Cs_xRb_{1-x}-Vm. Both systems exhibit a nonlinear $d_n(x)$ with approximate thresholds of $x \cong 0.2$ and 0.5, respectively. A model which related $d_n(x)$ to layer rigidity and the binding energies of gallery and defect sites yields excellent fits to the basal spacing data and to monolayer simulations if collective effects are included. This model should be applicable to other types of lamellar solids.

PACS numbers: 68.65.+g

Lamellar solids constitute a class of materials which exhibit a variety of specific properties. These properties are in large part determined by the host-layer transverse rigidity which characterizes its response to out-of-plane distortions.[1] For example, graphite, whose monatomic amphoteric layers are "floppy" and thus collapse around intercalated guest species, does not sustain a microporous structure with large internal surface area. In contrast, layered alumino-silicate "clays," whose multiatomic fixed-charge layers are "rigid," are unique among lamellar solids in their ability to be pillared[2] by robust intercalated guest ions which occupy specific lattice sites in the interlayer galleries.[3] The resultant pillared clay is characterized by widely spaced host layers that are propped apart by sparsely distributed guest species whose intralayer separation can be many times their diameter. The enormous free volume of accessible interior space that is derived from such an open structure has significant practical implications in the fields of catalysis and selective adsorption (sieving).

Although it is obvious that layer rigidity and pillaring, which is a special example of the more general phenomenon of intercalation, are interrelated, the pillaring mechanism has, to date, been poorly understood. For instance, none of the available elastic models account quantitatively for the full composition dependence of the the c-axis repeat distance of any intercalated layered solid.[4-6] It is not surprising that the rigid-layer versions of such models fail when applied to floppy or moderately rigid hosts such as graphite[5] and layer dichalcogenides.[5] But they are qualitatively inconsistent with data derived from clay hosts to which rigid-layer models should be most applicable. Accordingly, we report in this paper the first successful attempt to quantify and parametrize the relation between pillaring and layer rigidity. To accomplish this we have carried out x-ray and simulation studies of the x dependence of the basal spacing, $d(x)$, of mixed-layer vermiculite (Vm) clays A_xB_{1-x}-Vm, $0 \leq x \leq 1$, where A and B are cations (assume that A is larger than B) that are judiciously chosen to elucidate the physics of pillaring. In a previous study[6] we examined the Cs_xRb_{1-x}-Vm system for which the alkali intercalate species are best characterized as "puny" pillars since their ionic diameters are only 3.34 and 2.92 Å, respectively. Here we focus on the more robust mixed pillar system tetramethyl ammonium-trimethyl ammonium-vermiculite with effective diameters of 4.8 and 4.0 Å, respectively. We find that the pillaring process is a collective phenomenon which introduces an intrinsic nonlinearity in $d(x)$. While our results are deduced for clay intercalation compounds (CIC's) they should also be applicable to other lamellar solids.

Vermiculite is a trioctahedral 2:1 layered silicate. Its layers are formed from a sheet of edge-connected octahedra (M^{VI}=Mg, Al, Fe) which is bound to two sheets of corner-connected tetrahedra (M^{IV}=Si, Al) as shown in the inset of Fig. 1. The layers of oxygen atoms which terminate the clay layers are arranged in a *kagomé* lattice whose hexagonal pockets form a *triangular* lattice of gallery sites which here are constrained by the requirement of overall charge neutrality to be occupied by the gallery exchange cation. This occupation imposes a lateral registration of adjacent clay layers as indicated in the inset of Fig. 1. To synthesize the specimens studied here, the Mg^{2+} gallery cations which link the layers of natural Llano vermiculite were exchanged for $(CH_3)_3NH^+$ ions with ethylenediaminetetraacetate as a complexant.[7] Subsequent exposure of pure $[(CH_3)_3NH^+]$-Vm to the proper amount of $(CH_3)_4N^+$ yielded a solid-solution pillared CIC

$$[(CH_3)_4N^+]_x[(CH_3)_3NH^+]_{1-x}\text{-Vm}.$$

Self-supporting sedimented films exhibited a mosaic spread of $\simeq 5°$ with the layers parallel to the substrate.

The x dependence of the (00l) x-ray diffraction patterns of $[(CH_3)_4N^+]_x[(CH_3)_3NH^+]_{1-x}$-Vm is shown in Fig. 1. The starred reflections in that figure are from a small concentration of an impurity phase whose 14.477-Å basal spacing is x independent as evidenced by the vertical line in Fig. 1. The patterns in Fig. 1 can be well accounted for by a structure-factor calculation for a 25-layer stack.[7] We have also attempted to fit the pat-

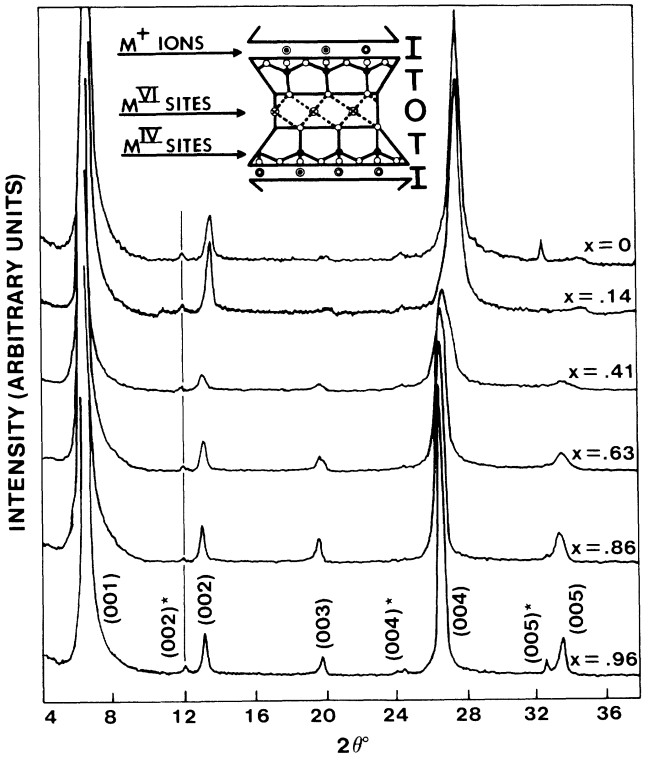

FIG. 1. Room-temperature x-ray diffraction patterns of $[(CH_3)_4N^+]_x[(CH_3)_3NH^+]_{1-x}$-Vm excited by Cu $K\alpha$ radiation (filled circles). Starred reflections are from an impurity phase. The solid vertical line shows the constant position of the (002)* reflection. Inset: Schematic structure of a 2:1 layered aluminosilicate clay with the tetrahedral (T) and octahedral (O) sheets which bound intercalated ions (I) (see text).

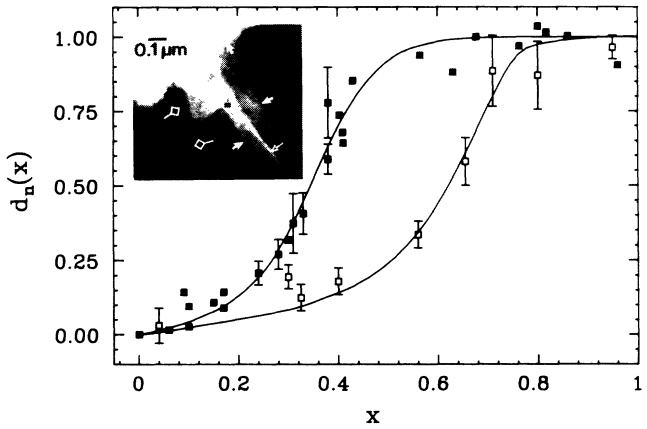

FIG. 2. The composition dependence of the normalized basal spacing of $[(CH_3)_4N^+]_x[(CH_3)_3NH^+]_{1-x}$-Vm (filled squares) and Cs_xRb_{1-x}-Vm (open squares). The solid lines are least-squares fits to the data with Eq. (4) of the text. Inset: Bright-field scanning-tunneling electron micrograph of $(CH_3)_3NH^+$-Vm acquired at $T=-135\,^\circ C$ with the electron beam normal to the layers. Note the free surface between layer edge dislocations (outline-headed arrows), the folded region (lozenges), and the microcrack (open-headed arrows). The small dotted grids are an instrumental artifact.

terns of Fig. 1 using a Hendricks-Teller (HT) model[8] for an interstratified structure.[7] The HT calculations yielded results which were clearly inferior to those based on a solid-solution arrangement in which all galleries have the same height. Moreover, a one-dimensional Patterson synthesis[9] from the measured peak intensities did not show any sign of interstratification.

From the data of Fig. 1, we have determined the x dependence of the normalized basal spacing,[6] $d_n(x)$ (or normalized c-axis repeat distance), of $[(CH_3)_4N^+]_x$-$[(CH_3)_3NH^+]_{1-x}$-Vm which is shown in Fig. 2 as filled squares. Here $d_n(x)=[d(x)-d(0)]/[d(1)-d(0)]$ where $d(x)$ is the observed basal spacing. Also shown in Fig. 2 for comparison are corresponding results for Cs_xRb_{1-x}-Vm (Ref. 6) (open squares). Both the Cs-Rb and $(CH_3)_4N^+$-$(CH_3)_3NH^+$ systems exhibit a non-Vegard's-law (nonlinear) rapid rise in $d_n(x)$ with increasing x at "threshold" values of $x_t=0.5$ and 0.2, respectively.

To understand the physical origin of the observed $d_n(x)$, we have simulated a model monolayer system with finite transverse layer rigidity. For simplicity we assumed that the intercalate ions are hard spheres. Starting from a two-dimensional triangular lattice of lattice constant a_0 representing a single gallery with each lattice site occupied by a B ion of height d_B, we randomly replace the B ions with A ions of height $d_A > d_B$. The height of a cell within a healing length λ of the A ion is also increased to d_A. A second A ion in this region does not affect already expanded cells but expands unexpanded cells within λ of its location. The process of random replacement of the B ions continues to saturation. If we define $\alpha(x)$ as the fraction of cells with height d_A, then $d_n(x)=\alpha(x)$. The simulation results for $d_n(x)$ are shown in Fig. 3 for several different healing lengths. Clearly, in the floppy-layer limit $\lambda=0$, a Vegard's-law behavior obtains whereas the initial slope $[d_n(x)]'_{x=0} \to \infty$ as $\lambda \to \infty$. As can be seen from Fig. 3, there is no percolation threshold even for finite λ because $d_n(x)$ depends upon all of the large ions, not only on those belonging to the infinite percolation cluster. Note that the nonlinearity in $d_n(x)$ for $\lambda > 0$ is a collective effect associated with the individual interaction between the larger ions through their distortion fields.

The sublinear x dependence and the rapid rise in $d_n(x)$ near x_t is outside the monolayer model. Several mechanisms including the relative magnitudes of host-guest and host-host interactions, interlayer correlations, and the presence of defect (d) sites can produce sublinear behavior in $d_n(x)$ but only the latter two can generate threshold effects. Since the ions of interest here are relatively incompressible we treat the guest species as hard spheres as noted above. The interlayer correlation mechanism is one in which large guest ions locally puck-

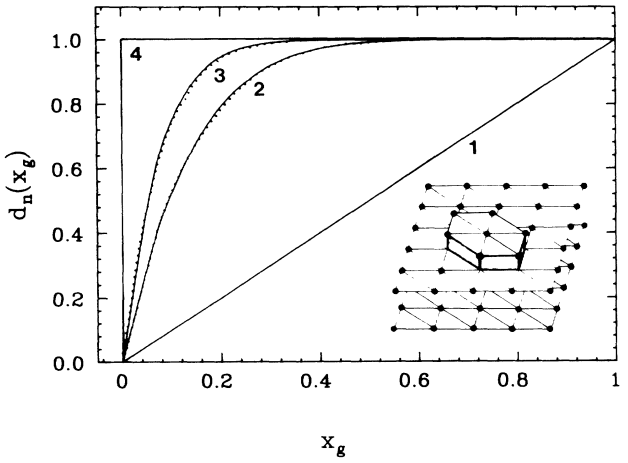

FIG. 3. Monolayer triangular lattice computer simulations (dotted lines) of the composition dependence of the normalized basal spacing of a ternary intercalation compound for several values of the healing length, λ, and rigidity parameter, p. The solid lines are from Eq. (4) of the text with (1) $p=1$, $\lambda=0$; (2) $p=7$, $\lambda=a_0$; (3) $p=13$, $\lambda=\sqrt{3}a_0$; and (4) $p=\infty$, $\lambda=\infty$. Inset: The puckered region of a triangular lattice with $\lambda=a_0$. Here the number of expanded sites is $p=Z+1=7$ where Z is the number of nearest neighbors.

er the bounding layers so that at low x they adopt staggered lateral positions, i.e., no line joining the centers of any pair of large ions in adjacent galleries is perpendicular to the silicate layer. This mechanism is relevant to host materials with low transverse layer rigidity such as graphite while the d-site mechanism is more appropriate to the more rigid layers of clays.

Sources of d sites in our specimens are shown in a scanning tunneling electron micrograph of $(CH_3)_3NH^+$-Vm (inset, Fig. 2). The region imaged consists of homogeneously intercalated areas (g sites) which are bounded laterally by layer edge dislocations and are capped by free surfaces (d sites) that bind guest species without inducing c-axis expansion. Since the clay grains have typical basal dimensions of a few micrometers, it is clear from the scale of the micrograph that these free surfaces can represent a significant fraction of the total surface available to guest species. Additional minor sources of d sites are the microcracks and folds that are visible in the micrograph.

We have explored the d-site mechanism by constructing a two-site model in which the basal spacing is assumed to depend upon the gallery A-ion concentration x_g which itself is a function of the total A-ion concentration x. The functional dependence of x_g on x is determined by two parameters, f and Δ/kT, where $f=N_d/N_g$ is the fraction of ions in d sites relative to those in g sites and Δ is the effective binding-energy difference between these sites, the d sites having a lower binding energy. For simplicity we assume only one type of d site. A statistical mechanics calculation gives

$$x_g=1/(z+1), \tag{1}$$

$$x=[1/(1+f)]x_g + [f/(1+f)]\{1/[z\exp(-\Delta/kT)+1]\}, \tag{2}$$

where $z=\exp[(\epsilon_g-\mu)/kT]$ is related to the fugacity and the binding energy ϵ_g of the g sites. Equations (1) and (2) can be solved to obtain $x_g=\phi(x,f,\Delta/kT)$ for different values of f and Δ/kT. Physically then for $x<x_t$, the A ions first preferentially displace B ions from the d sites. This reduces the gallery A-ion concentration for a given x and yields a sublinear increase in $d_n(x)$. For $x>x_t$ additionally ingested A ions enter the galleries. The result is a rapid increase in $d_n(x)$.

Using methods developed by Xia and Thorpe[10] one can obtain the following analytic solution for our monolayer simulation:

$$d_n(x_g)=1-(1-x_g)^p, \quad 0\le x_g\le 1, \tag{3}$$

where p is a layer rigidity parameter. This equation fits the simulation data extremely well as shown by the dotted lines in Fig. 3. For our lattice-gas simulation, $p=Z+1$ where Z is the number of neighboring sites that are puckered by the insertion of an isolated A ion (see inset Fig. 3). In the continuum limit ($\lambda\gg d_A/2$), $p\sim(2\lambda/d_A)^2$. Using Eq. (3) and $x_g=\phi(x,f,\Delta/kT)$, we obtain

$$d_n(x)=1-\{1-\phi(x,f,\Delta/kT)\}^p. \tag{4}$$

Note that the slope of $d_n(x)$ at $x\gtrsim x_t$ is governed by a combination of p and Δ/kT while x_t is determined primarily by f for large Δ/kT.

We have used Eq. (4) to obtain a nonlinear least-squares fit to the data of Fig. 2. The parameter values which give very good fits (solid lines in Fig. 2) for the two CIC systems $[(CH_3)_4N^+]_x[(CH_3)_3NH^+]_{1-x}$-Vm and Cs_xRb_{1-x}-Vm are $\{p=8.0, f=0.5, \Delta/kT=4.3\}$ and $\{p=7.0, f=2.2, \Delta/kT=4.1\}$, respectively. The smaller value of the rigidity parameter in the Cs-Rb system is consistent with the fact that alkali ions in CIC's can partially penetrate the bounding silicate layers. The mechanism which gives rise to this penetration is a torsional in-plane distortion[1,6] of the tetrahedral sheets which expands the hexagonal pockets that contain the guest species. Ion penetration of the clay layers causes a reduction of the apparent healing length. But the $(CH_3)_4N^+$ and $(CH_3)_3NH^+$ ions are much too large to penetrate the clay layer significantly, even in the presence of torsional distortions. Thus one expects the Cs-Rb-Vm system to exhibit a lower value of the rigidity parameter p. The f values deduced for the two systems also reveal interesting properties of the clay structure. For singly ionized guest species $N_j=\sigma A_j$ where σ is the layer charge density and A_j is the surface area asso-

ciated with j sites, $j=d,g$. If $A=A_d+A_g$ then $A_d=[f/(1+f)]A$ and $(A_d)_{Cs\to Rb}/(A_d)_{(CH_3)_4-(CH_3)_3}\cong 2$. Thus, of the surface which provides d sites for small Cs-Rb ions only about half (the portion not adjacent to edge dislocations, or derived from some microcracks or folds) can also accommodate the robust $(CH_3)_4N^+$-$(CH_3)_3NH^+$ ions without inducing basal expansion. Finally, the difference in the Δ/kT values for the two pairs indicates that the d sites are more attractive for the larger ions. This makes physical sense because the more spatially demanding ions prefer the less constrained defect environment to the more restrictive gallery.

The layer rigidity model which we have developed here should be directly applicable to other lamellar solids such as zirconium phosphates and layered niobates which have relatively rigid layers. It can also give insight into the behavior of intercalation compounds whose host layers have low or moderate rigidity. For example Li_xC_6 (Ref. 4) and Li_xTiS_2[11] exhibit no threshold in $d_n(x)$, and therefore contain few if any d sites. Also, there are conflicting reports of a Vegard's-law $d_n(x)$ for $Rb_xK_{1-x}C_8$ prepared from single-crystal graphite[12] and a thresholdlike sublinear behavior for the same compound prepared single-crystal graphite,[13] highly oriented pyrolytic graphite,[14] or powder.[15] For clay hosts sublinear threshold behavior can be reasonably associated with d sites. But for floppy-layer hosts such as graphite there is much evidence[15] that interlayer correlations and their associated strain fields dominate the behavior. Therefore, even though the non-Vegard's-law behavior of $Rb_xK_{1-x}C_8$ (Ref. 12) has been attributed to d sites, we do not believe that the model addressed here is applicable to that compound.

Finally, we have assumed that the site binding energies in our model are independent of concentration. This assumption might be relaxed if the binding energy of the g sites drops once the galleries are initially expanded. The resultant transfer of ions from d to g sites would then contribute to the rapid increase in $d_n(x)$ for $x\gtrsim x_t$.

We thank M. F. Thorpe for the derivation of Eq. (3). Useful discussions with H. X. Jiang and Y. B. Fan are acknowledged. This work was supported by the National Science Foundation under Materials Research Center Grant No. DMR 85-14154 and in part by the Center for Fundamental Materials Research of Michigan State University.

---

[a]Department of Chemistry.

[b]Department of Physics and Astronomy.

[1]S. A. Solin, in *Intercalation in Layered Materials,* edited by M. S. Dresselhaus (Plenum, New York, 1986), p. 145.

[2]T. J. Pennavaia, Science **220**, 365 (1983).

[3]Unlike graphite which is amphoteric, clays have a fixed layer charge. Intercalation in these materials is thus an intragallery ion-exchange process.

[4]There is one exception, $K(NH_3)_xC_{24}$, whose superlinear x-dependent basal spacing is qualitively distinct from that of clays but is well accounted for by a rigid-layer model which includes *both* elastic and electronic effects. See B. R. York and S. A. Solin, Phys. Rev. B **31**, 8206 (1985).

[5]J. E. Fischer and H. J. Kim, Phys. Rev. B **35**, 3295 (1987), and references therein.

[6]B. R. York *et al.,* Solid State Commun. **54**, 475 (1985).

[7]H. Kim *et al.,* to be published.

[8]S. Hendricks and E. Teller, J. Chem. Phys. **10**, 147 (1942).

[9]D. M. C. MacEwan, Nature (London) **171**, 616 (1953).

[10]W. Xia and M. F. Thorpe, Phys. Rev. A (to be published).

[11]J. R. Dahn, D. C. Dahn, and R. R. Haering, Solid State Commun. **42**, 179 (1982).

[12]D. Medjahed, R. Merlin, and R. Clarke, Phys. Rev. B **36**, 9345 (1987).

[13]P. Chow and H. Zabel, to be published.

[14]P. Chow and H. Zabel, Synth. Met. **7**, 243 (1983).

[15]S. A. Solin and H. Zabel, Adv. Phys. (to be published).

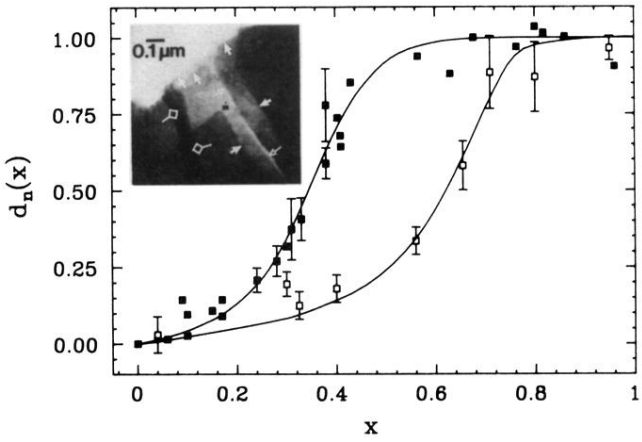

FIG. 2. The composition dependence of the normalized basal spacing of $[(CH_3)_4N^+]_x[(CH_3)_3NH^+]_{1-x}$-Vm (filled squares) and Cs_xRb_{1-x}-Vm (open squares). The solid lines are least-squares fits to the data with Eq. (4) of the text. Inset: Bright-field scanning-tunneling electron micrograph of $(CH_3)_3NH^+$-Vm acquired at $T=-135\,^{\circ}C$ with the electron beam normal to the layers. Note the free surface between layer edge dislocations (outline-headed arrows), the folded region (lozenges), and the microcrack (open-headed arrows). The small dotted grids are an instrumental artifact.

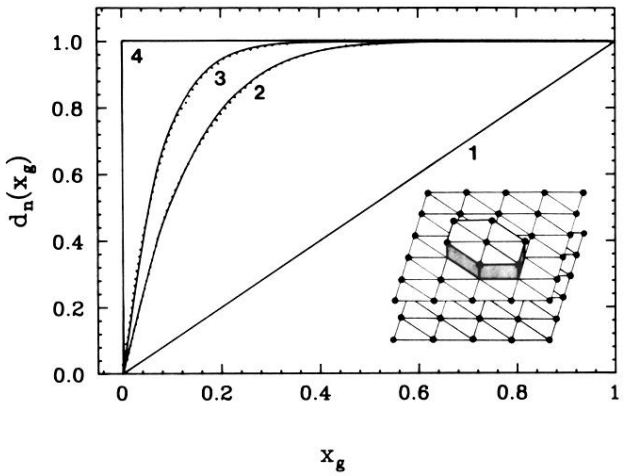

FIG. 3. Monolayer triangular lattice computer simulations (dotted lines) of the composition dependence of the normalized basal spacing of a ternary intercalation compound for several values of the healing length, λ, and rigidity parameter, p. The solid lines are from Eq. (4) of the text with (1) $p=1$, $\lambda=0$; (2) $p=7$, $\lambda=a_0$; (3) $p=13$, $\lambda=\sqrt{3}a_0$; and (4) $p=\infty$, $\lambda=\infty$. Inset: The puckered region of a triangular lattice with $\lambda=a_0$. Here the number of expanded sites is $p=Z+1=7$ where Z is the number of nearest neighbors.